Check for updates

Received: 17 February 2022 | Revised: 2 June 2024 | Accepted: 31 July 2024

DOI: 10.1111/jfr3.13029

ORIGINAL ARTICLE

CIWEM Chartered Institution of Water and Environmental Management | Journal of Flood Risk Management | WILEY

Assessment of urbanization-related groundwater flooding process via Visual MODFLOW modeling: A case study for the northern part of Almaty city, Kazakhstan

Vladimir Mirlas[1] | **Altynay Zhakyp**[2] | **Yergali Auelkhan**[2] | **Yaakov Anker**[1,3]

[1]Department of Chemical Engineering, Arial University, Ariel, Israel

[2]Department of Hydrogeology, Engineering and Oil and Gas Geology, Satbayev University, Almaty, Kazakhstan

[3]Department of Environmental Research, Eastern Israel R&D Center, Ariel, Israel

Correspondence
Yaakov Anker, Department of Chemical Engineering, Arial University, Ariel, Israel.
Email: kobia@ariel.ac.il

Abstract

Groundwater flooding might be triggered by disregarding hydrogeological processes during urban area development. Such flooding might result in public disruption, engineering infrastructure destruction, and general damage to natural and human environments, as in the northern part of Almaty city. A MODFLOW groundwater flow model was used to simulate and quantitatively assess the changes in hydrogeological conditions affecting the groundwater flooding process. A field study of the Akbulak micro-district research site showed that groundwater flooding occurred in its center owing to a water table hillock with a total area of 0.07 km^2 and groundwater levels ranging from 1.2 to 0.25 m below the ground surface. The MODFLOW simulation suggested that this water table hillock developed from runoff, which, owing to a decrease in natural infiltration across an urbanized area, accumulated in low-elevation areas and infiltrated. This runoff accumulation effect may be up to eight times the annual average precipitation amount. Once in local sub-basins, larger runoff volume infiltrates into an underlying aquifer water table that is already high, might cause groundwater flooding in populated areas. The Almaty scenario simulation confirmed the field observations, suggesting that the clogging of the Karasu-type stream has concentrated runoff to low-elevation areas and is the leading cause of flooding.

KEYWORDS

groundwater flooding, numerical modeling, rain-runoff infiltration, urban runoff

1 | INTRODUCTION

Flood risk management in the face of global climate change is shifting from the traditional approach of flood defense based on structural engineering solutions to a more dynamic approach of factorial flood risk management through scenario modeling. These models should consider global climate change-affected factors, such as sea level rise and rain potential, owing to air parcel water vapor carrying capacity (Ball et al., 2013). Moreover, the environmental feedback to anthropogenic factors of geological engineering and hydrogeological processes might result in losses of human life and property (Zou & Gui, 2020). While some natural hazards, such as

This is an open access article under the terms of the Creative Commons Attribution License, which permits use, distribution and reproduction in any medium, provided the original work is properly cited.
© 2024 The Author(s). *Journal of Flood Risk Management* published by Chartered Institution of Water and Environmental Management and John Wiley & Sons Ltd.

earthquakes and ground fissures, are not necessarily related to global climate change, desertification, water and soil pollution and degradation, water shortages (in some regions), flooding (in others), ground subsidence, landslides, and mudflows are known to be related (Azarafza & Ghazifard, 2016; Lara & Sepúlveda, 2010; Vakhshoori et al., 2019; Wu et al., 2021; Zarghami & Dumrak, 2021). Additional direct human impact threats include land use changes, waste, hazardous material incidents, pipeline accidents, and transportation effects (Skilodimou & Bathrellos, 2020).

Groundwater flooding might impact human well-being and economic activities through urban areas and household disruption and damage to public infrastructures and natural environments (Hughes et al., 2011). The dynamic and unpredictable nature of the situation is manifested by a significant increase in natural hazard insurance prices and the government funds allocated to restore disrupted urban areas that have suffered or are prone to suffering from catastrophic flood events (Ball et al., 2013). Urbanization changes the natural landscape by building accommodations and infrastructure, leading to an increase in impervious surface area and natural drainage network obstruction that aggravates flooding. This trend might be devastating where there are not enough drainage systems or available subsurface storage, resulting in groundwater flooding and direct runoff flooding (Fernández & Lutz, 2010).

The most dangerous groundwater flooding consequences occur in highly populated urban areas, such as the River Thames flood plains and tributaries around Oxford's metropolitan area (Aicha et al., 2020). However, good hydraulic connections to river canals mitigate groundwater flooding even when the sediments are saturated and groundwater levels are close to the ground surface (MacDonald et al., 2012). In the peri-urban area around Naples, Italy, features of flood-prone areas and groundwater flooding dynamics were mapped, providing a factorial groundwater flooding control analysis (Allocca et al., 2022).

Based on natural hazard element analysis in large Ukrainian cities, Chebanov and Zadniprovska (2011) created a thematic groundwater flooding risk map with zones of low, moderate, medium, high, and critical flood risks. Anker et al. (2019) assessed the effect of rapid urbanization on Mediterranean karstic mountainous drainage basins in Israel and indicated that to prevent flooding, urban areas should be planned with runoff infiltration zones to prevent hydrological effects on adjacent natural drainage systems. In addition to flood mitigation and groundwater recharge, the vacant land used as runoff-absorbing strata provides social benefits for the surrounding community (Pandit et al., 2020).

Global climate change was found to aggravate flash flooding by increasing the amount of water vapor in an air parcel. This trend has been addressed across China by sponge-city water-sensitive designs that mitigate runoff flooding until the phase of groundwater flooding. To mitigate groundwater flooding, natural drainage routes should be preserved and even modified (Wang et al., 2022). Another study from China indicated that deforestation causes a reduction in landscape roughness, which results in higher runoff peak flow and less infiltration, which, while reducing groundwater levels, aggravates runoff flooding (Xiong et al., 2020). Watershed lithological infrastructure has a direct effect on runoff and groundwater flooding; for example, karst infrastructure is less prone to flash flooding than silt and claystone infrastructures (Gao et al., 2021).

Models such as Building Information Modeling (BIM) are widely used for geologic hazard simulation and impact prediction (Zou & Gui, 2020). A three-dimensional numerical model of the Italian village of Ville San Pietro was used to evaluate damage-causing slope movements. This finite element code simulates the slope displacements and stability during water table fluctuations (Bovolenta & Bianchi, 2020). Su et al. (2020) studied the relationships among infiltration, sewer rehabilitation, and groundwater flooding to apply groundwater models simulating sewer replacement effects in coastal urban areas. Machine learning spatial distribution models employ aquifer type, groundwater level depth, unsaturated zone thickness, hydraulic conductivity, drainage density, land use, and groundwater observation data for groundwater flooding susceptibility assessment (Allocca et al., 2021). Yihdego et al. (2017) used the MODFLOW-SURFACT code to assess the spatial and temporal groundwater level rise and related groundwater flooding risks in a shallow, unconfined aquifer in Australia.

The present trend in hydrometeorological risk management is nature-based solutions, meaning that by modifying or not disturbing natural drainage systems, they can prevent flooding even in the current state of global climate change (Pandit et al., 2020). The problem emerges once urban development substitutes the flexible natural drainage system with a rigidly constructed system. To ensure an optimal interface between natural and human environments, numerical modeling is required to predict the anthropogenic effect on the natural hydrological system and the system's reaction based on human infrastructure endangerment. Few studies have achieved applicable modeling of such scenarios, which can assist stakeholder and planner decision-making, with a standard method remaining a distant goal (Kumar et al., 2021).

17533318x, 2025, 1, Downloaded from https://onlinelibrary.wiley.com/doi/10.1111/jfr3.13029 by INASP/HINARI - KAZAKHSTAN, Wiley Online Library on [05/04/2026]. See the Terms and Conditions (https://onlinelibrary.wiley.com/terms-and-conditions) on Wiley Online Library for rules of use; OA articles are governed by the applicable Creative Commons License

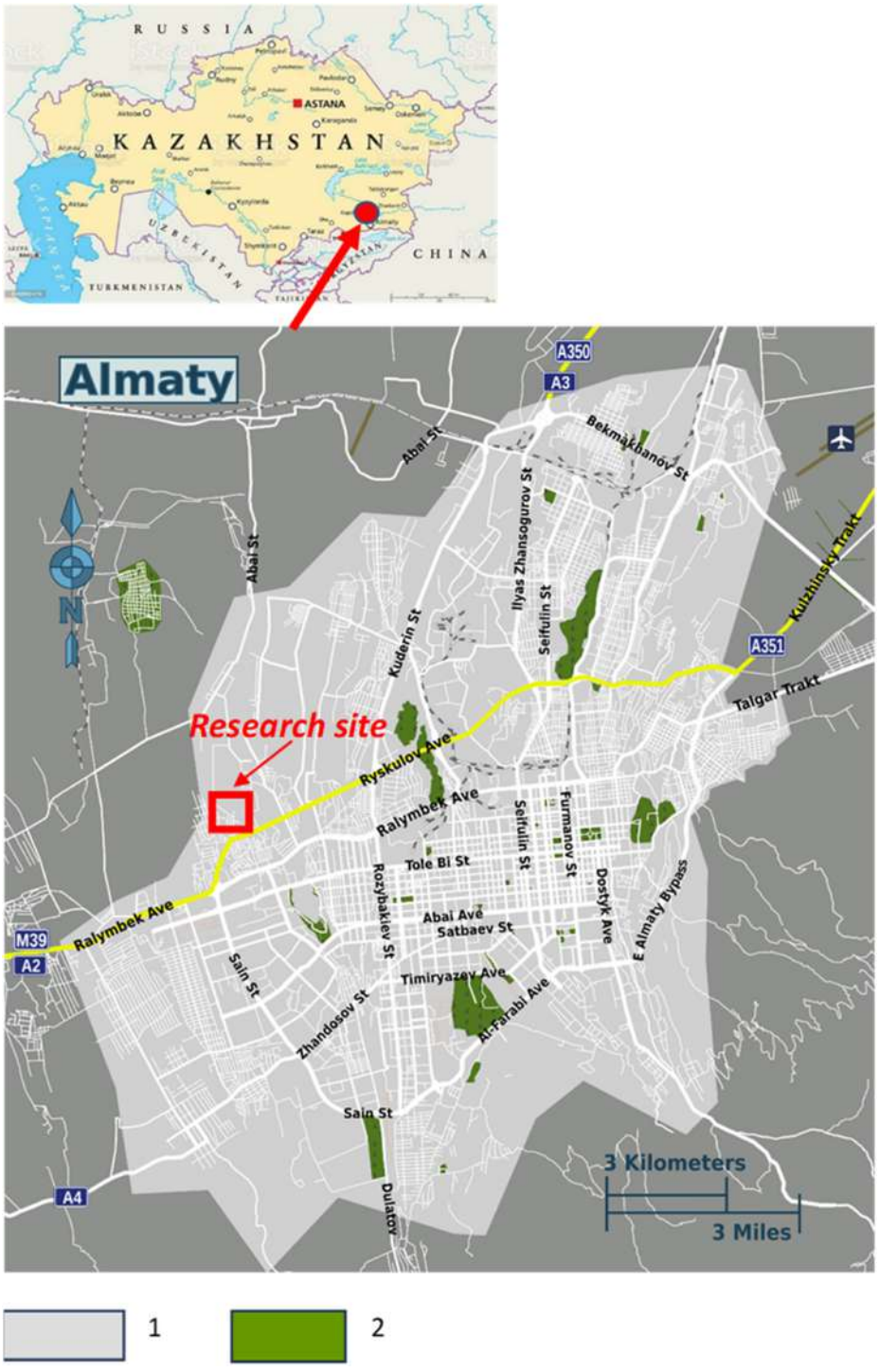


FIGURE 1 Groundwater flooding research site location. 1—The Almaty city parameter; 2—city gardens and parks. *Source*: https://commons.wikimedia.orG/wiki/File:Almaty_map.png.

The main research question is to understand how urbanization-related processes cause groundwater flooding, with the research hypothesis that urban development aggravates groundwater flooding. The research objective is to evaluate this hypothesis and establish a method to evaluate the real cost of various development alternatives from the perspective of flood mitigation strategy and potential flood damage. For that matter, aquifer hydrodynamic and water balance characteristics modeling is done under existing and future urban development scenarios. Groundwater flooding scenario assessment by numerical geo-filtration modeling involved the actual model development and validation.

The research site is a new neighborhood located in the northern part of Almaty that underwent development processes, including drainage regulation, during the last decade.

Geological and hydrogeological engineering hazards at the study site were evaluated and simulated, indicating that water flow energy is dictated by the pressure and

1753318x, 2025, 1, Downloaded from https://onlinelibrary.wiley.com/doi/10.1111/jfr3.13029 by INASP/HINARI - KAZAKHSTAN, Wiley Online Library on [05/04/2026]. See the Terms and Conditions (https://onlinelibrary.wiley.com/terms-and-conditions) on Wiley Online Library for rules of use; OA articles are governed by the applicable Creative Commons License



FIGURE 2 Research site Akbulak micro-district in 2021. Red—site boundary; blue—network of the Karasu streams that existed in 2021. The western stream is Boroldai Karasu (Google, 2021).

kinetic energy components of the water flow balance equation. Urban groundwater flooding in low-elevation areas in the northern plain of Almaty is a major hazard indicated by these simulations (Zhakyp et al., 2021).

1.1 | Geographical and hydrogeological setting of the research site

Almaty city is situated in the Ile Alatau foothill zone and is home to more than 1.5 million people. The city has a high density of industrial facilities, residential buildings, summer cottages, and a road network. Groundwater flooding hazards occur in the urban areas of the northern part of Almaty, which is located on the foothill plain of the Zailiyskiy Alatau Mountains. The Akbulak micro-district research site is in the northwestern part of the city, north of Ryskulov Street between Boroldai Karasu (stream) in the west and Sagi Ashimov Street in the east; in the north, it is limited by Shugaly Street (Figures 1 and 2). The experimental site boundaries were chosen so that it was possible to include all the main factors that determine the groundwater flooding process, such as land use shifts during urban area development, changes in

1753318x, 2025, 1, Downloaded from https://onlinelibrary.wiley.com/doi/10.1111/jfr3.13029 by INASP/HINARI - KAZAKHSTAN, Wiley Online Library on [05/04/2026]. See the Terms and Conditions (https://onlinelibrary.wiley.com/terms-and-conditions) on Wiley Online Library for rules of use; OA articles are governed by the applicable Creative Commons License

TABLE 1 The average long-term water flow rate for 50% probability of the main rivers in Almaty after (Chigrinets et al., 2019).

River	Watershed area, km^2	Observation period, year	Water flow rate, m^3/s
Kargaly	44.9	1938–1941, 1944–1961, 1963–1983	0.60
Ulken Almaty	155	1990–1998, 2004–2006, 2008–2011	0.97
Kishi Almaty	118	1974–2011	1.82
Esentai	28.0	1965–1974	0.06
Zharbulak	-	1963, 1976–1980	0.79

groundwater recharge and discharge conditions, and well data monitoring the dynamics of water withdrawal from underlying aquifers. In this regard, this experimental site allows new quantitative and qualitative information about the groundwater flooding process in northern Almaty to be obtained.

The climate in the region is hot and dry and can be regarded as transitional from arid to semi-arid, with hot and dry summers and an average annual temperature of just +9°C owing to cold and mildly snowy winters. A maximum air temperature of +42°C is usually recorded in July and August, and the minimum temperature of −38°C occurs in January. Climate change in the region has manifested as a temporal temperature increase trend of 1.4°C since 1970 (Cherednichenko et al., 2015). The annual precipitation varies from 290 to 550 mm, whereas 140–170 mm is recorded in April–May. The multi-year average annual open water evaporation potential is 1500 mm, with approximately one-third (436 mm) occurring during the hottest month (August) (Chigrinets et al., 2019).

The study area is part of the Ily River drainage basin, the region's main waterway. The Ily River is the local drainage datum for five main streams (Kargaly, Ulken Almaty, Kishi Almaty, Esentai, and Zharbulak), and numerous tributaries flow down from the snow and glacial melt over the northern slope of the Zailiysky Alatau Ridge through the Almaty area. In terms of the average long-term flow of these rivers, 50% is from the mountains to the submontane talus of the Zailiyskiy Alatau (Table 1).

The water of these rivers is calcium carbonate with a total dissolved salt concentration varying from 0.069 to 0.16 g/L. Upon leaving the mountains, the river flow is filtered into alluvial fan loose sediments (talus morena), which is a local aquifer supplying potable and irrigation water through a dense canal network. The local terminology for spring-fed streams (in addition to snowmelt and runoff) with gradually increasing baseflow owing to groundwater seepage is known as "Karasu." The Karasu-type streams originate at the transition of the alluvial fan to the foothill plain, with the hill aquifer discharge zone manifested in numerous springs (Figure 3). The Karasu stream regime is constant throughout the year, and the total dissolved salt concentration does not exceed 0.3 g/L, which is attributed to calcium carbonate and sodium carbonate.

In 1974, the Almaty alluvial fan area measured a total maximal groundwater flow rate of 3.6 m^3/day (Akhmedsafin et al., 1978). The groundwater flooding of buildings and other engineering structures following this event was attributed to the topographic leveling of some Karasu streams and the regulative actions of others, which decreased the natural drainage capacity (Akhmedsafin et al., 1978).

Almaty city is located in the southern part of the Ily Hydrogeologic Artesian Basin, where the mountains bordering the Ily intermountain depression are the basin's recharge areas (Akhmedsafin et al., 1980). Quaternary deposits inconsistently lying on Neogene clays are the main water-bearing sediments, forming a single alluvial fan aquifer complex divided into several hydrodynamically interconnected confined aquifers above the foothill plain. Hydrostatic heads increase with depth, which indicates groundwater vertical discharge and recharge of the upper horizons with waters of the deeper aquifers. The Quaternary sediment thickness ranges from 500 to 600 m in the central part of the alluvial fans and from 200 to 300 m on the foothill plain.

The decrease in the total thickness of the Quaternary alluvial sediment is compensated by increasing the thickness of the loamy layer, which significantly reduces the groundwater flow cross-sectional area and aquifer transmissivity. As a result, part of the flow is discharged (wedged out), forming numerous springs, which feed the Karasu-type streams and swamps on the foothill plain.

The groundwater flow direction correlates with the ground surface gradient from the mountains to the Ily River valley. The groundwater depth varies from 200 m at the alluvial fan top to several meters at the foothill periphery. The alluvial fan aquifer complex comprises boulder-pebble deposits with a gravel-sand matrix. The maximal transmissivity values (up to 12,500 m^2/day) are typical for the lower part of the fans. The hydraulic

1753318x, 2025, 1, Downloaded from https://onlinelibrary.wiley.com/doi/10.1111/jfr3.13029 by INASP/HINARI - KAZAKHSTAN, Wiley Online Library on [05/04/2026]. See the Terms and Conditions (https://onlinelibrary.wiley.com/terms-and-conditions) on Wiley Online Library for rules of use; OA articles are governed by the applicable Creative Commons License



FIGURE 3 Boroldai Karasu flows across the western boundary of the research site. (a) Springs at the beginning of the Karasu; (b) Boroldai Karasu in the northern part of the research site. Photo taken by A. Zhakyp in 2020.

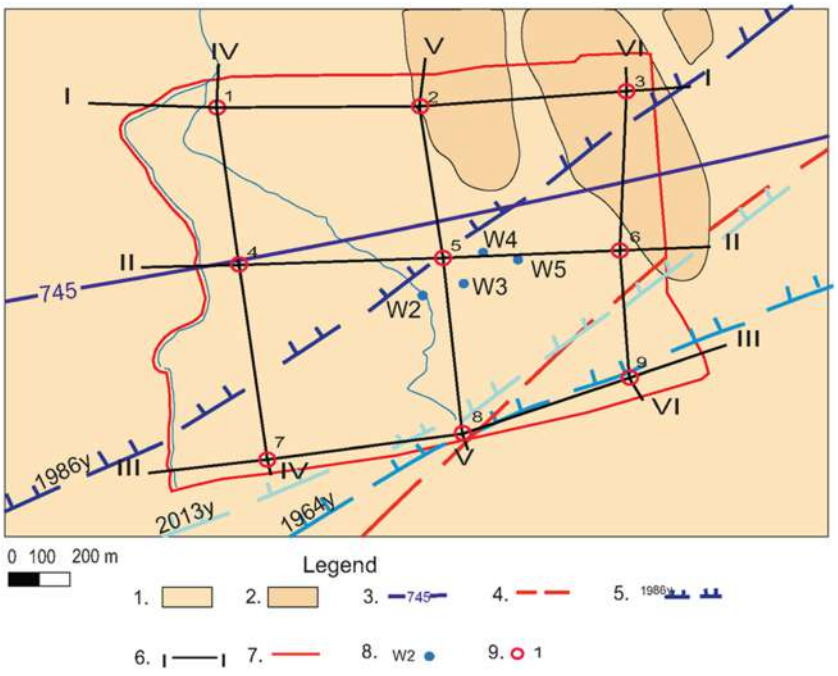


FIGURE 4 Hydrogeological zoom map of the Akbulak micro-district research site (Abisheva & Yambaev, 2017). 1. (apQ_{III})—Upper Quaternary alluvial-proluvial aquifer. Pebbles, gravel-pebble and gravelly sands with interlayers of sandy clays; 2. (apQ_{II})—Middle Quaternary alluvial-proluvial water-bearing complex. Boulder-pebbles, gravel-pebbles, and sands with interlayers of sandy clays; 3. Groundwater head contours of the upper aquifer; 4. Deep faults under loose overlying sediments; 5. Groundwater wedging out zone boundary according to observation year; 6. Hydrogeological cross-section and its number; 7. Research site boundary; 8. Observation well; 9. Hydrogeological borehole.

conductivity values and effective porosities vary from 28 to 100 m/day and 0.2 to 0.3, respectively (Akhmedsafin et al., 1978). The specific discharge of the pumping wells is 30–40 L/s, with actual discharge of 100–200 L/s under a 3–5 m drawdown. The groundwater is a calcium carbonate type with a total dissolved salt concentration of 0.2–0.3 g/L.

The "Akbulak micro-district" research site is geomorphologically located on an alluvial-proluvial foothill plain (Figure 4). In lithological terms, the research site is confined to the Upper Quaternary alluvial-proluvial deposits (apQ_{III}). Water-bearing sediments comprise gravel-pebble and gravelly sands, with a typical granulometric composition of clay particles—1.3%; silt—2.9%; sand—39%; and gravel—57.8%. The medium-grained sand consists of clay particles—0.8%; silt—4.3%; sand—59.1%; and gravel—35.8% (Zhakyp et al., 2021). Due to this lithological composition, the hydraulic conductivity values do not exceed 15–20 m/day. The specific discharge of pumping wells is 1.5–3.0 L/s for a 1 m drawdown, with

1753318x, 2025, 1, Downloaded from https://onlinelibrary.wiley.com/doi/10.1111/jfr3.13029 by INASP/HINARI - KAZAKHSTAN, Wiley Online Library on [05/04/2026]. See the Terms and Conditions (https://onlinelibrary.wiley.com/terms-and-conditions) on Wiley Online Library for rules of use; OA articles are governed by the applicable Creative Commons License



FIGURE 5 Urbanized areas and the Karasu stream network at the "Akbulak micro-district" research site. (a) 1967, (b) 2021. 1—undeveloped areas; 2—urban areas; 3—Karasu stream and its number; 4—swamps and wetland areas.

an actual water flow rate during pumping from wells of 50–70 L/s under a 30–40 m drawdown.

The water supply of Almaty city has relied on groundwater since 1960, with a gradual increase in groundwater uptake from 62,500 m^3/day in 1960 to 1,006,000 m^3/day (approximately 16 times higher) in 1986. Subsequently, the total average annual water uptake stabilized at approximately 940,000 m^3/day, and the total water uptake decreased from 760,000 m^3/day in 1993 to 605,000 m^3/day in 2002. From 2002 to 2014, the average annual groundwater uptake was 640,000 m^3/day (Sotnikov & Ibraimov, 2017). Almaty's groundwater supply system is located approximately 15 km from the lower boundary of the alluvial fans and consists of 166 pumping wells, which are grouped into 26 nests. In the foothill plain area (northern part of Almaty), there are six additional groundwater pumping sites, with 10–18 wells in clusters with 10–100 m between the wells. The well flow rates are in the range of 30–60 L/s, from a depth range of 150–500 m. Infrastructural deterioration between 1992 and 2000 reduced groundwater uptake, but since 2000, old well recovery actions and the drilling of new wells have constantly increased groundwater uptake.

The increase in water withdrawal during 1969–1975 caused a sharp groundwater level drawdown, with an overall increase from 1960 to 1996 of 23.6 m on the alluvial fan and 26.9 m on the foothill plain. As a result, spring seepage in the Karasu streams changed from 6.0 m^3/s in 1960 to 2.08 m^3/s in 1988. The Karasu stream's starting point was displaced 2.0 km further north from the alluvial fan. During the 2005–2007 period, groundwater levels started to rise until the current groundwater level stabilized. Within this trend, the groundwater wedging out zone boundary moved south

1753318x, 2025, 1, Downloaded from https://onlinelibrary.wiley.com/doi/10.1111/jfr3.13029 by INASP/HINARI - KAZAKHSTAN, Wiley Online Library on [05/04/2026]. See the Terms and Conditions (https://onlinelibrary.wiley.com/terms-and-conditions) on Wiley Online Library for rules of use; OA articles are governed by the applicable Creative Commons License

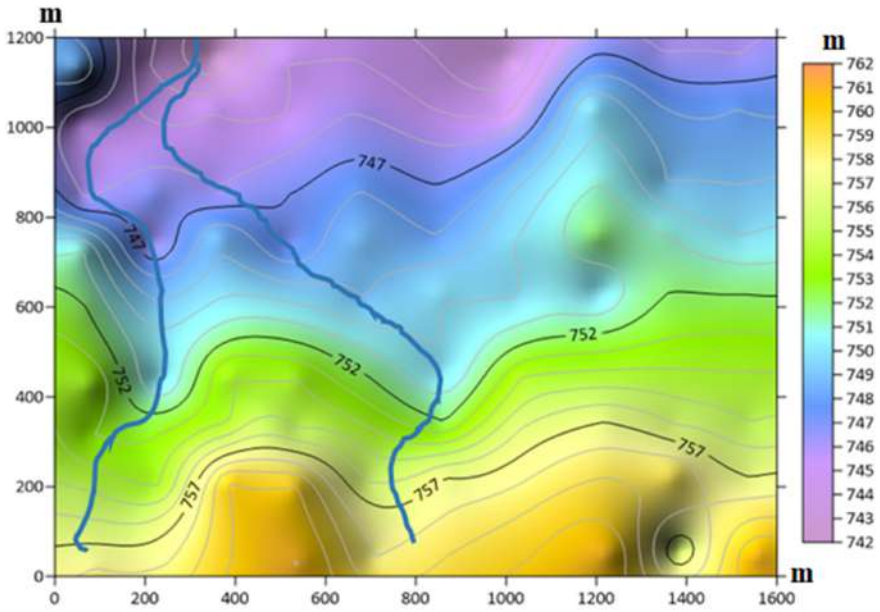


FIGURE 6 The surface elevation in 2021 (created by Surfer 13 software).

toward the alluvial fans (Figure 4). The increase in groundwater level due to the reduction in water withdrawal in the northern part of Almaty city led to groundwater flooding in urban areas.

The intensive urban area development in the city's northern part included relief leveling and filling the Karasu valleys with low-permeability sediments. Changes in the urban areas and the Karasu stream network around the research site from 1967 to the present are shown in Figure 5. The urban areas increased from 0.18 to 1.81 km^2 and are currently 62.8% of the total research site area (2.88 km^2). The remaining open areas consist of some Karasu riverbeds and homestead areas between buildings (gardens, vegetable gardens, squares, and side streets). Some are in low-elevation areas and represent potential zones of urban runoff infiltration. Of the 12 Karasu streams flowing through the research site in 1967, only two remained: Boroldai Karasu, which flows along the western boundary (number 1 in Figure 5), and its inflow at the central part of the study site (number 7).

The surface leveling during regional development in 2021 is shown in Figure 6, and local depressions in the topography are also clearly visible and can serve as runoff concentration areas.

2 | MATERIALS AND METHODS

2.1 | Modeling setup

The basic assumption is that the pre-urban physiographic areas, such as the Karasu stream watershed, are obstructed by urban development, particularly in the northern part of Almaty city. This increase in impervious surfaces results in greater runoff volume and peak discharge and causes groundwater flooding. The specific research hypothesis is that the Karasu channel clogging concentrates runoff to low-elevation infiltration areas, which causes a groundwater hillock that elevates the groundwater table around these areas and motivates groundwater flooding. To evaluate the groundwater flooding process, computer modeling was integrated with field measurements to calculate the upper unconfined aquifer hydrodynamic and water balance coefficients, which affect groundwater flooding processes. The evaluation of the model's lower boundary initial groundwater heads considered water withdrawal from the alluvial fan aquifers during the last decade and modeled groundwater interactions with the underlying deeper confined aquifers. The modeling approach was applied to the study site rather than the entire region since, to attain sufficient accuracy, the necessary basic information should be at a volume that enables model construction and validation to be coherent with its solutions. Correct boundary conditions are essential for determining the simulated process dynamics, particularly the groundwater recharge and discharge conditions that change in time and space.

2.1.1 | Hydrogeological survey

A hydrogeological survey was conducted to evaluate the groundwater dynamics parameters that are required for geo-filtration modeling. The hydrogeological survey included the following:

1. Drilling and installation of four observation piezometers (indicated by the letter W in Figure 4), each 15 m

1753318x, 2025, 1, Downloaded from https://onlinelibrary.wiley.com/doi/10.1111/jfr3.13029 by INASP/HINARI - KAZAKHSTAN, Wiley Online Library on [05/04/2026]. See the Terms and Conditions (https://onlinelibrary.wiley.com/terms-and-conditions) on Wiley Online Library for rules of use; OA articles are governed by the applicable Creative Commons License

deep. All piezometers were equipped with a slit filter and gravel filling perforation at a depth interval of 9–11 m. The main criteria for choosing the observation well locations were the susceptibility of these areas to periodic groundwater flooding after floods and heavy rains and the existing building conditions at the research site.

2. Groundwater level monitoring in the four monitoring wells was performed every 10 days from April 15, 2017 to April 15, 2019. The frequency of groundwater level measurements was set under the current guidelines (Mavritskii et al., 1983) and existing practices for monitoring groundwater levels in Kazakhstan. The selected measurement frequency provided an objective and reliable reproduction of the groundwater level fluctuations dynamics with the required accuracy and minimum possible number of measurements.
3. On May 18, 2020, the Karasu stream water flow rate measurement was carried out by flow velocity measurement using hydrometric mechanical reels in temporary gaging stations, including flow source mapping within the research site.
4. The field measurement database included rainfall and evaporation potential measured at the Almaty airport meteorological station and groundwater level measured at nearby observation piezometers. The database also included geological-technical logs of more than 40 wells drilled since 1990 at the research site and around it by different geological and hydrogeological organizations.

The field measurement database was used for spatial analysis of the different parameters required to create and calibrate the groundwater flow model, such as boundary conditions, the absolute height of the model layer surfaces, hydraulic conductivity, groundwater levels in the observation wells, recharge, and the location of the low-elevation area in which runoff infiltration was concentrated. Matrix distributions of these parameters in the database were used as input files for the Visual MODFLOW model.

2.1.2 | The site computer modeling structure

Based on the geological-technical borehole logs, six intersecting geological and lithological cross-sections were constructed (Figure 4). Figure 7 shows the filtration scheme for the V-V hydrogeological cross-section (Figure 4) of the central part of the research site. The filtration scheme, compiled on its basis, is a three-layer 3_D model consisting of two aquifers and one separating a relatively weakly permeable interlayer (aquitard).

The mathematical model represented the groundwater flow using a partial differential equation of groundwater flow through porous media in a three-layer geo-filtration system consisting of an upper unconfined aquifer, a middle confined low-permeability layer, and a lower confined aquifer.

For the upper unconfined aquifer, the flow equation is as follows:

$$\frac{\partial}{\partial x}\left[Kx(Hx-\eta x)\left(\frac{\partial H}{\partial x}\right)\right]+\frac{\partial}{\partial y}\left[Ky(Hy-\eta y)\left(\frac{\partial H}{\partial y}\right)\right]\pm W=\mathrm{Sy}\left(\frac{\partial H}{\partial t}\right). \quad (1)$$

For the lower confined aquifers, the flow equation is as follows:

$$\frac{\partial}{\partial x}\left[Kx\left(\frac{\partial H}{\partial x}\right)\right]+\frac{\partial}{\partial y}\left[Ky\left(\frac{\partial H}{\partial y}\right)\right]\pm W=\mathrm{Ss}\left(\frac{\partial H}{\partial t}\right), \quad (2)$$

where Kx and Ky are hydraulic conductivity along the x- and y-coordinate axes, respectively, which are the principal permeability directions; H is the potentiometric head; ηx and ηy are the elevations of the bottom of the unconfined aquifer along the x- and y-coordinate axes, respectively; W are the fluxes that represent the recharge, evaporation, and pumping wells, respectively; Sy is the specific yield of the porous material; Ss is the specific storage of the porous material; and t is the time. Equations (1) and (2), with the boundary conditions below and an initial head condition specification, provided a mathematical model representation of the groundwater flow for the study area.

The model boundary conditions are described in Section 2.1.3. To represent the spatial variability of the experimental site, the area was overlaid with a grid, with each cell representing a point in the center of that cell. The grid was applied to the layer that characterized the hydrodynamic and geological changes through the soil cross-section. The "Akbulak micro-district" research site groundwater model was constructed using Visual MODFLOW Pro v. 4.1 of Schlumberger Water Services software, which is an integrated computer program package for three-dimensional groundwater flow simulations based on physical laws of groundwater flow and mass transport in porous media. It is a widely used software package due to its easy access, relatively low cost, user-friendliness, and capability for transient/steady groundwater flow, simulating complex hydraulic conditions with various natural hydrological processes and/or artificial activities (Sanford, 2002). Visual MODFLOW can calculate flow fluxes across cell boundaries and

1753318x, 2025, 1, Downloaded from https://onlinelibrary.wiley.com/doi/10.1111/jfr3.13029 by INASP/HINARI - KAZAKHSTAN, Wiley Online Library on [05/04/2026]. See the Terms and Conditions (https://onlinelibrary.wiley.com/terms-and-conditions) on Wiley Online Library for rules of use; OA articles are governed by the applicable Creative Commons License

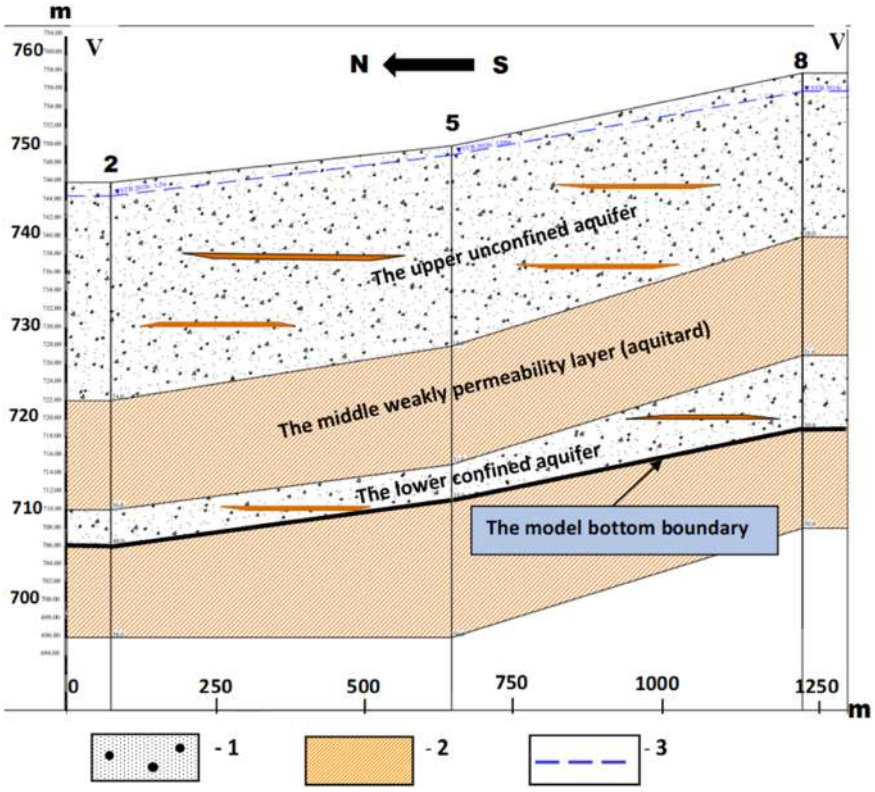


FIGURE 7 Hydrogeological cross-section V–V (Figure 4) of the central part of the research site. 1—Water-bearing sediments (gravel-pebble and gravelly sands); 2—low-permeability sediments (loamy layers with gravelly sand lenses); 3—groundwater level of the upper unconfined aquifer.

groundwater balances for different zones and predict groundwater head distributions in space and time. Hence, the Visual MODFLOW software package was selected for the present study. Groundwater head map contours and groundwater level depths from the soil surface were created using the MODFLOW software package's instrumental identification and task-solving capabilities (Schlumberger Water Services, 2011).

2.1.3 | Model illustration

A computer model of the experimental site was created within the boundaries that reflect the hydrological local sources and sinks of the study site: the western model boundary runs along the Boroldai Karasu riverbed, the southern boundary runs along the Ryskulov St., the northern boundary runs along the Shugyla St. from Boroldai Karasu to Sagi Ashimov St., and the eastern border of the model stretches along Sagi Ashimova St. from its intersection with Shugyla St. to Ryskulov St. (Figure 1).

Following the approval of the mathematical model, a computer model consisting of three horizontal layers was built for the Quaternary unconfined and confined aquifers. The bottom boundary of the model was the roof of the loam layer representing an aquiclude, which was adopted as an impermeable boundary and divided the model layers from the underlying pumped aquifers (Figure 8).

The three-layered model represents the field cross-section as follows:

Layer 1 represents unconfined upper aquifer thickness that ranges from 15 to 30 m, composed of Quaternary sand and gravel deposits with thin lenticular sandy-loamy interlayers.

Layer 2, with a thickness that varies from 4 to 15 m, represents the low-permeability aquitard layer separating the upper and lower aquifers, consisting of lenses and thin layers of sandy loam and loam as well as gravel-sand deposits with a sandy-loamy matrix. This layer induces hydrostatic head difference between the aquifers and groundwater overflow between the layers.

Layer 3 (lower) represents the underlying semi-confined sandy-pebble aquifer, which is 15–20 m thick. Its groundwater heads are located mainly near the surface of the day.

The model area was divided into a rectangular grid with 55 × 56 computational cells (3080 in total) for each model layer. The grid steps along the axes were uneven and varied from 20 to 81 m along the x-axis and from 16 to 63 m along the y-axis. Thus, the maximal computing cell area was 5103 m^2, and the minimum was 320 m^2. The minimal computational grid step was applied for the site area itself, where detailed information was needed. The model coordinate origin was in the lower-left corner

1753318x, 2025, 1, Downloaded from https://onlinelibrary.wiley.com/doi/10.1111/jfr3.13029 by INASP/HINARI - KAZAKHSTAN, Wiley Online Library on [05/04/2026]. See the Terms and Conditions (https://onlinelibrary.wiley.com/terms-and-conditions) on Wiley Online Library for rules of use; OA articles are governed by the applicable Creative Commons License

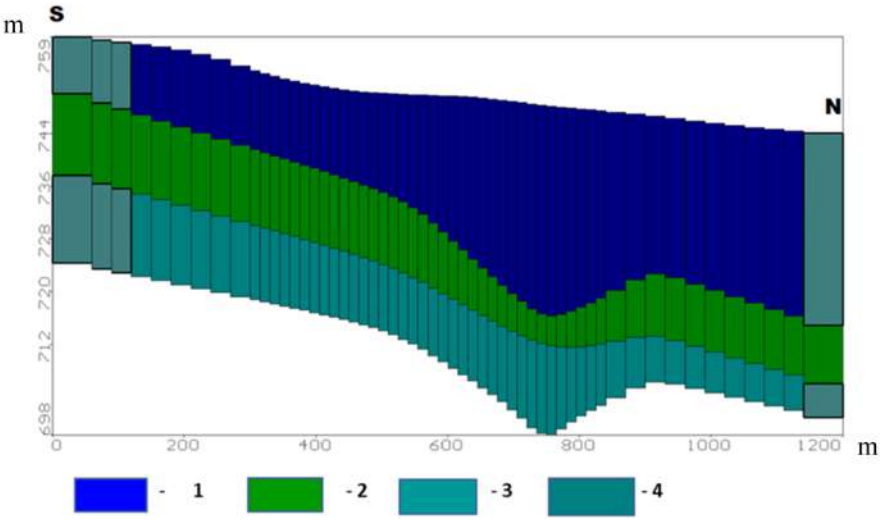


FIGURE 8 Model cross-section of the central part of the "Akbulak micro-district" research site with a schematic demonstration of the lithological layers in the model cells. 1—unconfined aquifer (first) layer of the model, down from the ground surface; 2—aquitard (second) layer of the model; 3—leaky confined aquifer (third) layer of the model; 4—inactive (non-computed) blocks in the model that are outside the outer boundaries of the model and the experiment zone.

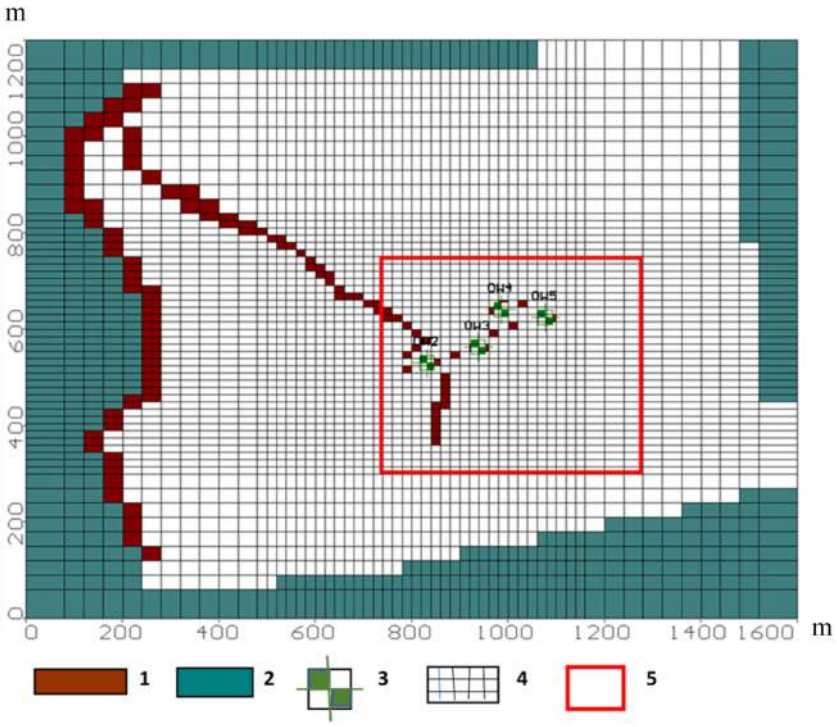


FIGURE 9 The "Akbulak micro-district" research site: First layer model grid and boundary conditions. 1 = boundary condition, first type; 2 = inactive cells (no flow within the model domain); 3 = observation well; 4 = active cells; 5 = detailed (representative) area.

of the rectangular region and corresponded to the point of intersection of Ryskulov St. with Boroldai Karasu (Figure 1). Defining inactive blocks outside its external borders emphasized the actual geo-filtration area configuration.

The model boundary conditions, reflecting the main factors that determine the groundwater flooding process, are defined for the upper (first) layer of the model (Figure 9):

1. Karasu-type stream: Defined with first type boundary conditions (specified constant head, $H = h(t)$, where h—the head at the boundary is given).
2. Precipitation infiltration from April to November, as recharge in the model is blocked.
3. Evapotranspiration: Defined as a third type boundary condition (head-dependent flux, $q = \mathrm{ET}(h - D)$, where ET is the maximal evapotranspiration, h is the groundwater head, and D is the extinction (critical) groundwater depth on which ET = 0).

The close hydraulic connection between the groundwater level and the Karasu stream water level was assessed as a boundary condition of the first type (BC-I), with a pressure head that matched the bottom surface in the Karasu riverbed and, accordingly, a volume change.

1753318x, 2025, 1, Downloaded from https://onlinelibrary.wiley.com/doi/10.1111/jfr3.13029 by INASP/HINARI - KAZAKHSTAN, Wiley Online Library on [05/04/2026]. See the Terms and Conditions (https://onlinelibrary.wiley.com/terms-and-conditions) on Wiley Online Library for rules of use; OA articles are governed by the applicable Creative Commons License

The groundwater spatial recharge from rainfall and irrigation was entered as an input to the Visual MODFLOW Recharge Package (Schlumberger Water Services, 2011), where groundwater recharge is 8.5% of the mean annual precipitation (470 mm/year), which for a foothill plain was set in the model as 40 mm/year (Akhmedsafin et al., 1978, 1980, 1982). The total groundwater recharge value was subsequently adjusted at the calibration and model validation stages.

The groundwater table contribution to evaporation and evapotranspiration was calculated by the Visual MODFLOW Evaporation Package (Schlumberger Water Services, 2011), whereas the capillary fringe boundary condition assumes a linear relationship between evapotranspiration potential and groundwater level. The groundwater withdrawal was calculated for each time step for the specific groundwater level depth. The evapotranspiration and evaporation maximal values were calculated for the groundwater level at the surface. With decreasing groundwater level, the evapotranspiration flux also decreased linearly up to a depth of 1.5 m, where it was null (Alemie et al., 2019). The initial local meteorological evaporation values were uniform across the model area, with a critical depth corresponding to the prevailing lithological composition of the vadose zone. As the mean long-term water evaporation value around the study site is 1500 mm/year, the water evaporation values were set with a monthly average from April to November, which varied from 147 mm/year for November to 2185 mm/year in July (Chigrinets et al., 2019).

Since the groundwater head data of the semi-confined aquifer at the model boundary are spatially and temporally irregular, no boundary conditions were set for this layer. The hydrodynamic groundwater flow grid was based on groundwater head contour maps that were combined with flow paths. The maps were built on May 25, 2018, when the highest groundwater level and groundwater flooding at the research site were observed.

2.1.4 | Model calibration and validation

During the calibration stage, the model was adjusted until it closely simulated the measured historical functioning of the modeled system. The model parameters for layer hydraulic conductivity values, aquifer storage coefficients, and recharge were manually adjusted, and the water balance was evaluated. Since there were no steady-state hydrodynamic conditions since the 1970s to represent the pre-urbanized area, only non-steady-state (time-varying) phases were modeled. The model was run from January 1, 2017 to January 1, 2020, during which the actual system behavior was observed. The model was run with time steps that were automatically chosen by the Visual MODFLOW program. However, where the simulated water level and pressure behavior did not match the observed behavior, careful manual adjustments were progressively made to the model's hydraulic conductivity, and layer recharge values were assigned to characterize the relevant cells.

Model calibration continued until a close match between the simulated and observed behaviors was achieved. The measured and calculated accuracy levels of coincidence should not exceed 0.2 m, which was possible owing to the detailed delineation of the lithological section and the precision of the spatial discretization. Considering that the groundwater level fluctuation amplitude in the observation wells reached 1.5 m, the declared accuracy cannot exceed 15%. The water balance coincidence and geo-filtration parameters obtained from field measurements were used for model validation. Large areas were sealed during regional development, preventing direct rain infiltration, which concentrated surface runoff into the drainage systems to low-elevation areas. Replacing distributed recharge with an equal concentrated runoff infiltration value at points in low-elevation areas was necessary. The recharge values at these points were adjusted during the calibration stage. Since this information was inconsistent across the entire study area, model identification was performed in a limited (representative) area adjacent to the observation wells (Figure 9).

3 | RESULTS AND DISCUSSION

3.1 | Model calibration

The model sensitivity analysis results under various parameters indicated that the model could recognize changes in specific storage (initial values of 30%) and the hydraulic conductivity of the layers. The model was more sensitive to recharge, showing that with the initial values of the hydraulic conductivity coefficient and recharge, the groundwater levels were 1.5–2.0 m lower than those recorded in the observation wells. A change in the hydraulic conductivity and specific storage values within the first order values (±10 times) had practically no effect on the calculated groundwater levels. As a result, the hydraulic conductivity values of observation wells OW2, OW3, and OW4 were reduced in the upper model layer from 15 to 0.1 m/day and in the second layer from 0.1 to 0.0001 m/day. It was found that even a threefold increase in recharge over the area does not lead to a groundwater

1753318x, 2025, 1, Downloaded from https://onlinelibrary.wiley.com/doi/10.1111/jfr3.13029 by INASP/HINARI - KAZAKHSTAN, Wiley Online Library on [05/04/2026]. See the Terms and Conditions (https://onlinelibrary.wiley.com/terms-and-conditions) on Wiley Online Library for rules of use; OA articles are governed by the applicable Creative Commons License

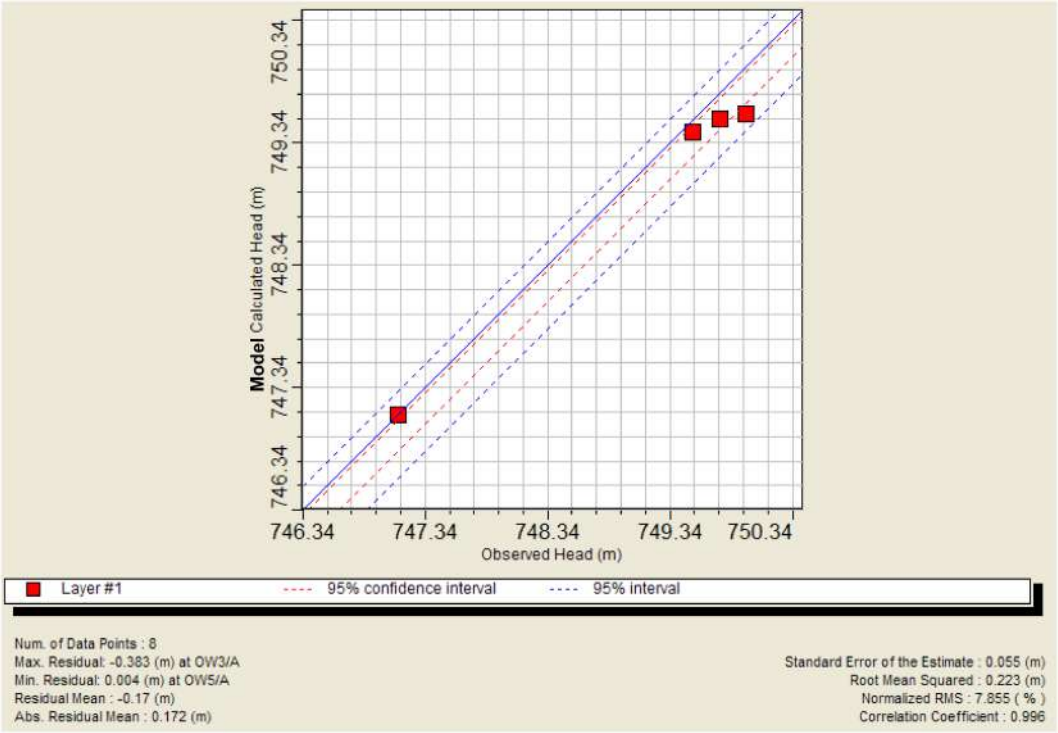


FIGURE 10 Comparison between model-calculated and measured average groundwater levels in the observation wells.

rise up to the groundwater levels required by the model to initiate flooding. The groundwater level fluctuation regime in the observation wells was simulated by setting first type boundary conditions with time-varying heads according to the measured groundwater level in the observation wells (Figure 8). The groundwater recharge values at these points were then calculated using the Visual MODFLOW balance module.

Based on the sensitivity analysis results, reducing the model parameter uncertainty and equifinality was possible. The main selection criteria of the water-bearing complex and groundwater recharge ranges were the geological relations to the hydraulic conductivity values and specific storage, which were based on the results from earlier studies in this region (Akhmedsafin et al., 1978, 1980, 1982; Sotnikov & Ibraimov, 2017), as well as the groundwater flow balance model calculation analysis. As a result, the hydraulic conductivity decreased around observation wells OW2, OW3, and OW4 in the upper model layer from 15 to 0.1 m/day and in the second layer from 0.1 to 0.0001 m/day. A comparison of the groundwater heads measured in the observation wells and the model-calculated heads showed sufficient agreement (Figure 10). The residual mean was 0.17 m, the absolute residual mean was 0.172 m, the estimated standard error was 0.055 m, and the root mean square (RMS) was 0.223 m. In addition, the correlation coefficient between the measured and modeled groundwater levels was 1.0.

A comparison of the measured groundwater level fluctuations and the model-calculated fluctuations revealed good agreement (less than ±0.4 m) between the observed and modeled results for the observation wells (Figure 11).

3.2 | The hydrodynamic and water balance characteristics of the groundwater flow at the research site (modeling results)

The general direction of groundwater flow in the upper unconfined aquifer coincides with the geological slope in a northerly direction toward the research site's northwestern corner to the main groundwater recharge area into the Karasu River (Figure 12).

The draining influence of the Karasu stream in the research site center was reduced during local development, causing an expanding water table hillock and groundwater flooding of buildings. A detailed groundwater head contour map and flow for the representative area demonstrates this scenario in Figure 13.

The height of the water table hillock in the central part, near observation well OW3, was 2.5 m and varied from 1.5 to 2 m along its long axis. The water table hillock, in the form of a curved ellipse, stretches along the long axis by approximately 300–350 m, and in the transverse direction, its dimensions are 200–220 m. A comparison of urbanized areas between 1967 and 2021 (Figure 5)

1753318x, 2025, 1, Downloaded from https://onlinelibrary.wiley.com/doi/10.1111/jfr3.13029 by INASP/HINARI - KAZAKHSTAN, Wiley Online Library on [05/04/2026]. See the Terms and Conditions (https://onlinelibrary.wiley.com/terms-and-conditions) on Wiley Online Library for rules of use; OA articles are governed by the applicable Creative Commons License

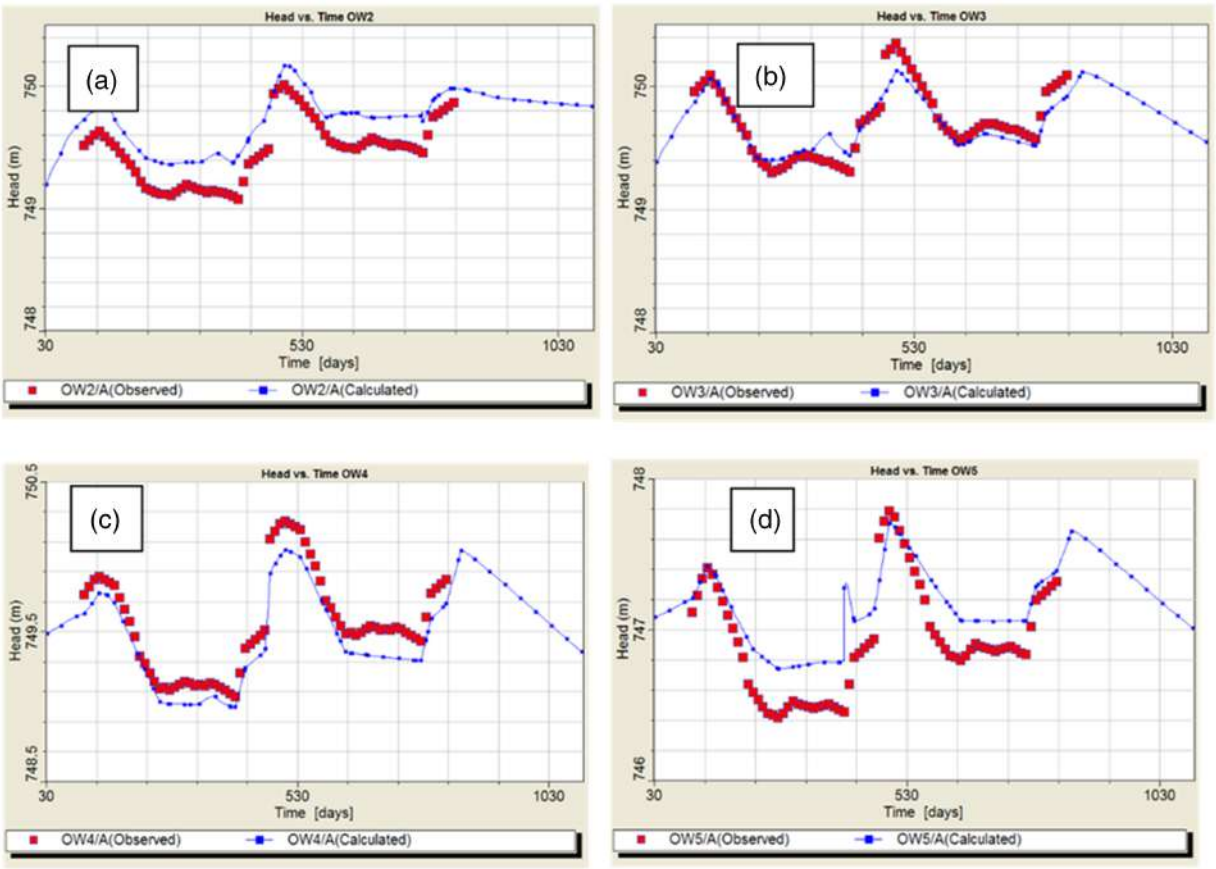


FIGURE 11 Model calibration versus observed groundwater head fluctuations in the observation wells (OW), January 2017 to January 2020. (a) OW2; (b) OW3; (c) OW4; (d) OW5. Red line—observed head; blue line—calculated head.

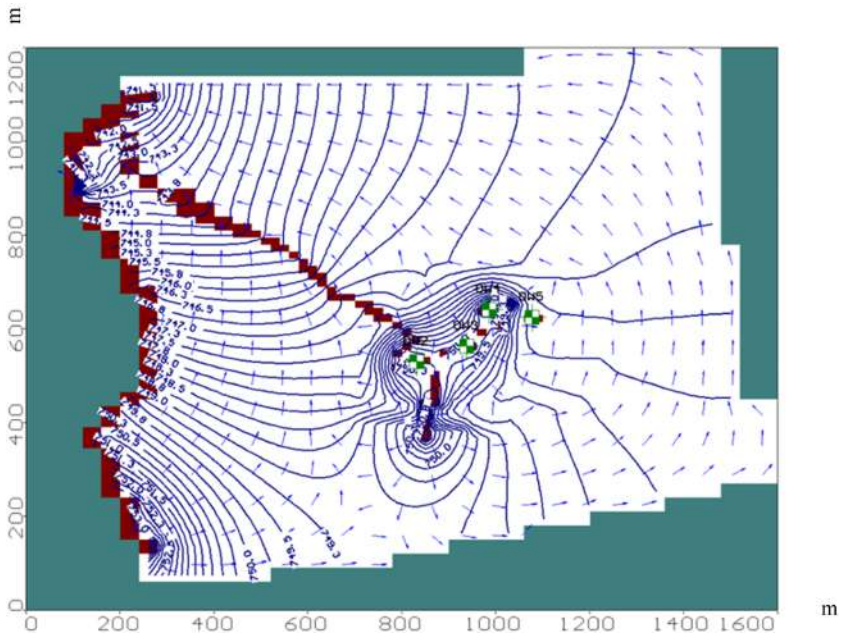


FIGURE 12 Groundwater head contours and flow path in an unconfined aquifer, May 25, 2018 (the highest groundwater level during the observation period).

shows that the zone of maximum groundwater level rise is confined to the swamp area and follows the progress in natural groundwater flow conditions, which explains the low filtration properties of the aquifer in this local area. In addition, these areas are characterized by a depression (Figure 6) and serve as places where surface runoff is

1753318x, 2025, 1, Downloaded from https://onlinelibrary.wiley.com/doi/10.1111/jfr3.13029 by INASP/HINARI - KAZAKHSTAN, Wiley Online Library on [05/04/2026]. See the Terms and Conditions (https://onlinelibrary.wiley.com/terms-and-conditions) on Wiley Online Library for rules of use; OA articles are governed by the applicable Creative Commons License

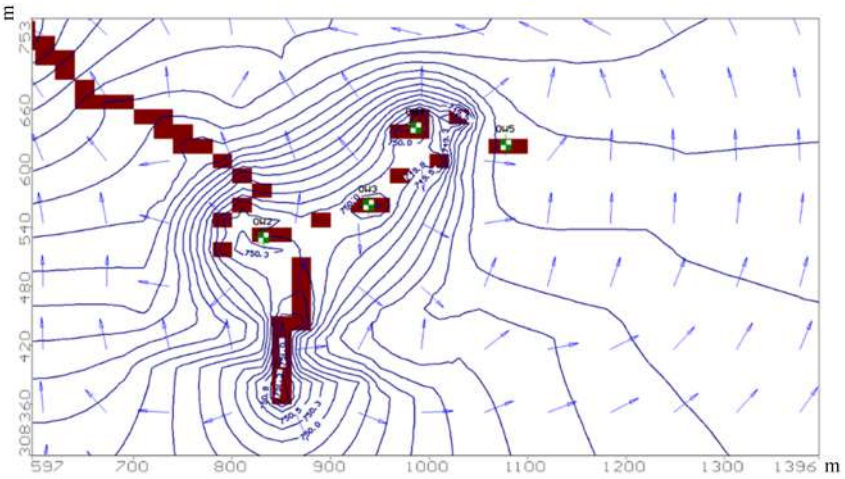


FIGURE 13 Groundwater head contours and flow paths in the unconfined aquifer in the detailed (representative) area May 25, 2018.

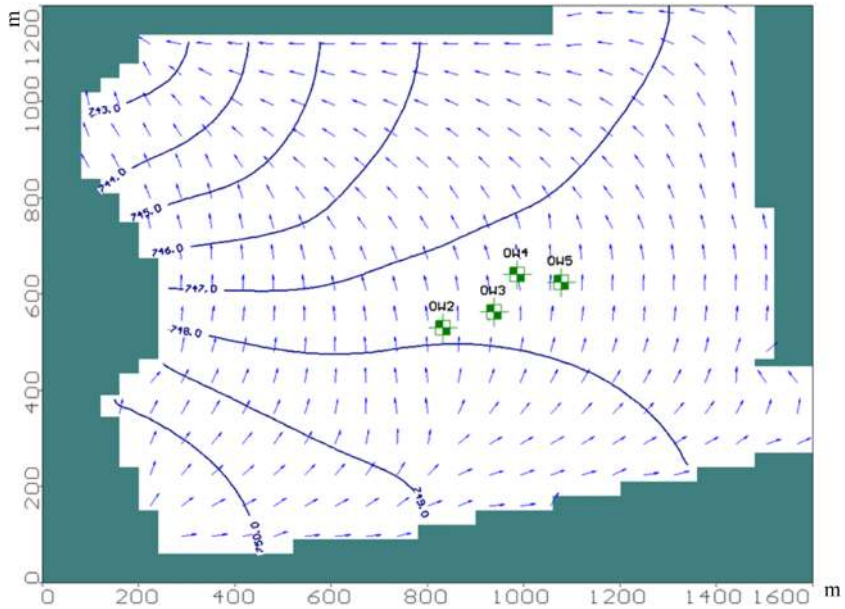


FIGURE 14 Groundwater head contours and flow path in the weak pressure confined aquifer, May 25, 2018.

concentrated from urbanized areas. The general northwest groundwater flow direction in the lower semi-confined aquifer coincides with the unconfined groundwater flow direction (Figure 14).

The influence of the (upper) aquifer water table hillock decreased the hydraulic gradient in the groundwater flow direction in the representative (detailed) area. Vertical overflow during the highest groundwater level through a slightly permeable layer separating the upper confined aquifer and the lower confined aquifers is shown in Figure 15 as groundwater levels and groundwater head variations that characterize the hydrodynamic connection between aquifers.

Areas with positive differences between groundwater level and head elevation (head values above the groundwater level) are characterized by an upward groundwater overflow and are found in areas of intense discharge into the Karasu streams in the northwestern corner of the research site. At most of the research sites, there is practically no difference between the groundwater level and head. Around the water table hillock, at the runoff seepage points into the sub-confined aquifer, the groundwater level is significantly higher than the head elevation, and groundwater overflow occurs. The groundwater depth at the research site varied from 10 to 1 m or less (Figure 16).

The maximal groundwater surface depth occurs at the site's southern border due to groundwater drawdown from pumping. In the rest of the study region, the depth varied from 4 to 2 m, whereas in the infiltration area, hillock development reduced the groundwater depth to less than 1 m. The groundwater level monitoring data at the observation wells indicated that groundwater decreased from the end of September to March. A comparison between the model for the highest (May 25, 2018) and lowest (February 15, 2018) groundwater levels

1753318x, 2025, 1, Downloaded from https://onlinelibrary.wiley.com/doi/10.1111/jfr3.13029 by INASP/HINARI - KAZAKHSTAN, Wiley Online Library on [05/04/2026]. See the Terms and Conditions (https://onlinelibrary.wiley.com/terms-and-conditions) on Wiley Online Library for rules of use; OA articles are governed by the applicable Creative Commons License

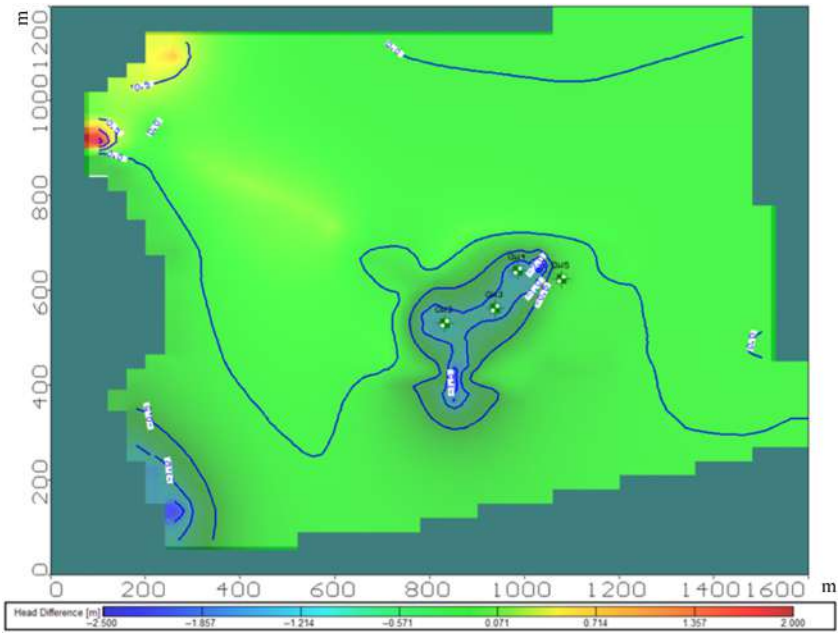


FIGURE 15 The difference in groundwater levels (first layer) and groundwater heads of a semi-confined aquifer (third layer), May 25, 2018.

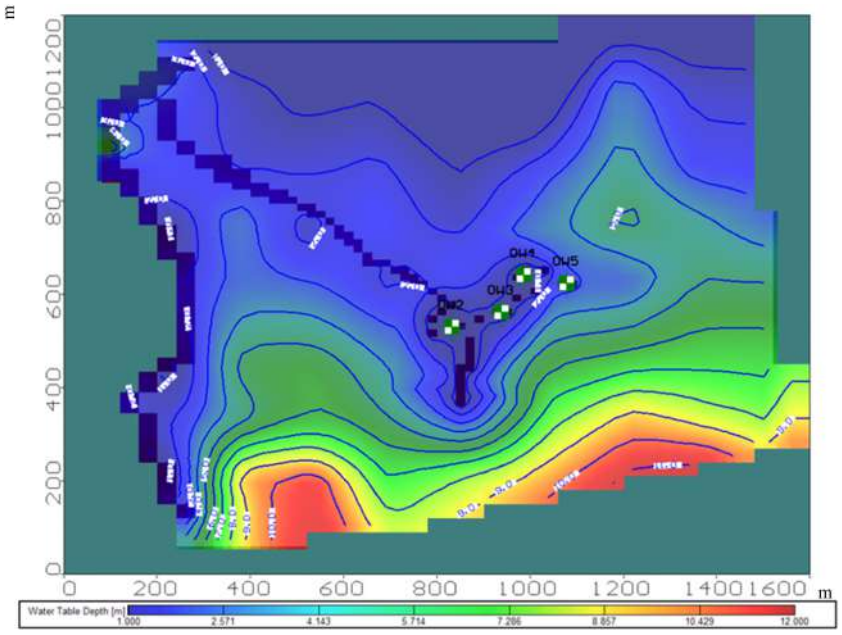


FIGURE 16 Groundwater depth, May 25, 2018.

indicated fluctuations within 0.5 m across most of the research sites. Within the central part of the representative area, the groundwater depth increased from February to 1.5 m above the ground, causing a water table hillock. No runoff concentration was observed in areas confined by the Karasu streams, and the groundwater table depth remained less than 0.5 m even during the autumn–winter period.

The groundwater-flux balance model (Table 2) suggested that the total groundwater flow rate at the "Akbulak micro-district" research site, which includes the upper and semi-confined aquifers, was 5145 m^3/day.

Pumping that caused a decrease in groundwater head reduced the inflow from the alluvial fans at the southern boundary of the research site to slightly more than 2%; runoff filtration from the Karasu streams contributed up to 57% of the groundwater inflow, and the rest was attributed to direct runoff infiltration from precipitation (4%) and groundwater from other boundaries. The groundwater flow input from the representative area of the research site was 23.4%, whereas the groundwater recharge from runoff infiltration reached 11%. The groundwater discharge into the Karasu streams is the most significant (approximately 80% of the sum of the

1753318x, 2025, 1, Downloaded from https://onlinelibrary.wiley.com/doi/10.1111/jfr3.13029 by INASP/HINARI - KAZAKHSTAN, Wiley Online Library on [05/04/2026]. See the Terms and Conditions (https://onlinelibrary.wiley.com/terms-and-conditions) on Wiley Online Library for rules of use; OA articles are governed by the applicable Creative Commons License

TABLE 2 Groundwater-flux balance at the "Akbulak micro-district" research site for May 25, 2018. Results of the model calculation.

Balance items		m^3/day	% from total
Input	Storage recharge	84	1.6
	Infiltration of precipitation	216	4.2
	Groundwater inflow from the southern boundary	123	2.4
	Infiltration from Boroldai Karasu	1140	22.1
	Infiltration from Karasu in the central part of the site	1802	35.2
	Groundwater inflow from the representative area	1206	23.4
	Infiltration runoff on the representative area	574	11.1
Total input		5145	100
Output	Evapotranspiration	388	7.5
	Discharge to Boroldai Karasu	2522	48.9
	Discharge to Karasu in the central part of the site	1586	30.8
	Groundwater outflow to representative area	202	3.9
	Groundwater outflow to the southern boundary	105	2.0
	Groundwater outflow to the northern boundary	350	6.9
Total output		5154	100
Input–output		−9	−0.04

output balance components). The groundwater outflow through the site's northern border accounted for 7%, and the remainder was due to evapotranspiration (approximately 8%) and outflow to the representative area.

The groundwater flow balance suggested that the total groundwater flow rate was 1290 m^3/day and did not change during the year. An overwhelming part of the total groundwater flow rate (78% of the sum of the input components) is formed due to runoff infiltration. The groundwater inflow from the outer representative area boundaries was 15%, and the remaining 7% of the groundwater flow rate was formed due to direct precipitation infiltration and filtration from the Karasu streams. The groundwater flow balance indicated that most of the flow was accounted for by groundwater seepage as runoff outside the representative area (93.5%). The evapotranspiration was 3%, and the remainder (3.5%) was discharged into the Karasu streams. Thus, the water table hillock spreading under the representative urban area was formed merely from surface runoff infiltration to low-elevation areas.

The representative area and groundwater flow balance model made it possible to quantitatively estimate the groundwater recharge from specific places of runoff accumulation. In total, 13 blocks were set with first type boundary conditions for simulating runoff accumulation and infiltration over a total area of 5200 m^2. The groundwater recharge due to surface runoff infiltration increased to 50–70 m^3/day in the spring, followed by a decrease to 10–30 m^3/day in the autumn–winter period (Figure 17).

Over the 3-year observation period, there was a slight upward trend in the minimum flow rate. The calculated groundwater infiltration recharge varied from 10.5 to 2.5 mm/day, with precipitation ranging from 3832 to 912 mm/year. The maximum recharge value from infiltration indicated by the model in different locations exceeded the precipitation amount (470 mm/year) by more than eight times, and the minimal recharge value exceeded the precipitation amount by almost twofold.

4 | CONCLUSIONS

The changes in the Almaty urban area and the Karasu stream network may symbolize a common interface between urbanized natural areas and their natural drainage system that is altered as part of urban development actions (Anker et al., 2019). In the northern part of the city of Almaty, such a trend caused groundwater levels to rise, and groundwater flooding started at local sites. The engineering-geological and hydrogeological processes causing groundwater flooding resulted from a decrease in groundwater pumping in the groundwater intake zones at the southern boundary of the study site. This highly dynamic process depends on the water intake and its total discharge regime (Akhmedsafin et al., 1978; Sotnikov & Ibraimov, 2017). The decrease in the dynamic

17533 18x, 2025, 1, Downloaded from https://onlinelibrary.wiley.com/doi/10.1111/jfr3.13029 by INASP/HINARI - KAZAKHSTAN, Wiley Online Library on [05/04/2026]. See the Terms and Conditions (https://onlinelibrary.wiley.com/terms-and-conditions) on Wiley Online Library for rules of use; OA articles are governed by the applicable Creative Commons License

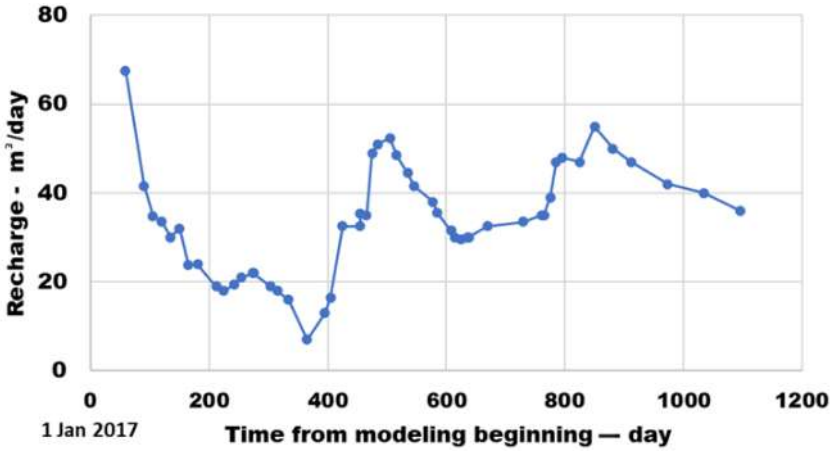


FIGURE 17 The modeled groundwater recharge is due to surface runoff infiltration from the representative area.

groundwater heads in the underlying confined aquifers was found to be related to the overlying aquifer groundwater levels and the semi-confined aquifer (lower layer of the model). The "Akbulak micro-district" was selected as a research site for understanding the groundwater flooding process, including groundwater level monitoring carried out during 2017–2020 and the design of a modeling platform for that scenario.

The groundwater depth in the observed wells varied from 1.2 to 0.25 m below the surface during the observation period. The highest groundwater level during the observation period was attained on May 25, 2018 at the center of the research site, where groundwater urban area flooding was noted. A water table hillock developed in a total area of at least 0.07 km^2. These field observations were used for training, testing, and calibration of a MODFLOW model built to clarify the local aquifer system's hydrodynamic and water balance characteristics that motivate the groundwater flooding processes.

The modeling results imply the following:

1. The MODFLOW spatial distribution groundwater flow model provided a reliable illustration of groundwater flow in the upper phreatic and sub-confined aquifers and through the separating aquitard between them. The model solution's accuracy and reliability meet the modeling objectives.
2. The model enabled recreating the current groundwater conditions, with regional urbanization and the Karasu network's partial clogging as well as water withdrawal by production wells. The Karasu network piping, which decreased the natural drainage on the southern boundary of the study site, was the cause of groundwater flooding in the residential areas (Figure 4). The development of urbanized areas in the northern part of Almaty city increases the total volume of urban runoff, which causes a rise in the groundwater level. In general, the existing urban drainage systems that replaced the Karasu stream channels had insufficient capacity, which caused runoff accumulation and infiltration in low-elevation areas (Figure 5), which aggravated groundwater flooding and might also be a source of groundwater contamination.
3. Based on the simulation results for May 25, 2018, which was the highest groundwater level during the 2018–2020 observation period, detailed groundwater head contour maps, flow paths, and groundwater table depths were generated. The groundwater transfer between the modeled aquifers, as indicated by the maps of the pressure differences between them, enabled the identification of groundwater recharge and discharge areas that caused groundwater flooding at specific locations across the research site, and the groundwater levels were high.
4. A groundwater flow balance model was prepared for a representative area where groundwater level monitoring was carried out and then extrapolated to the entire research site. The groundwater flow temporal balance trend suggests that runoff is diverted and concentrated in low-elevation areas due to urbanization. This runoff accumulation effect may reach eight times the annual precipitation amount (from 900 to 3800 mm/year), forming a water table hillock and leading to flooding.
5. The hypothesis that altering natural drainage networks through urban development degrades a watershed's hydrological tolerance to climate change-motivated extreme events was confirmed in this experimental study. The field monitoring results and MODFLOW simulation show that filling and regulating the natural Karasu network decreases drainage and, together with the insufficiency of existing urban drainage systems, leads to groundwater flooding in populated areas.

1753318x, 2025, 1, Downloaded from https://onlinelibrary.wiley.com/doi/10.1111/jfr3.13029 by INASP/HINARI - KAZAKHSTAN, Wiley Online Library on [05/04/2026]. See the Terms and Conditions (https://onlinelibrary.wiley.com/terms-and-conditions) on Wiley Online Library for rules of use; OA articles are governed by the applicable Creative Commons License

Storm sewers and underground drainage, which divert storm runoff from low areas and Karasu stream preservation and permeable valleys fill during development, can serve as the best basis for drainage management to prevent groundwater flooding in northern Almaty in the future.

CONFLICT OF INTEREST STATEMENT

The authors declare no conflict of interest.

DATA AVAILABILITY STATEMENT

The dataset used for the modeling is available at DOI: 10.17632/fh2yg5nymw.1.

ORCID

Yaakov Anker https://orcid.org/0000-0003-4747-0774

REFERENCES

Abisheva, K. S., & Yambaev, I. M. (2017). Groundwater supply resources reassessment exploration of Alma-Ata. Report on the results of geological exploration work on revaluation of groundwater reserves of the Alma-Ata deposit for water supply of Almaty city with calculation of reserves as of 01.01.15, carried out in 2013-2015 (Russian). State municipal enterprise "Bastau", Department of Energy and Public Utilities, Almaty municipality, Almaty, 859 p.

Aicha, O., Abdessamad, G., & Hassane, J. O. (2020). Groundwater flooding in urban areas: Occurrence process, potential impacts and the role of remote sensing and gis techniques in preventing it. In *Proceedings – 2020 IEEE International Conference of Moroccan geomatics MORGEO* (Vol. 2020). IEEE. https://doi.org/10.1109/Morgeo49228.2020.9121879

Akhmedsafin, U., Mirlas, V., S. V., & Shestakov, F. (1978). *Formation, forecasting and control of ground water resources in foothills* (Z. Sydykov, Ed.) (Russian). Alma-Ata, USSR: Publishing House "NAUKA". https://armunicat.nla.am/cgi-bin/koha/opac-detail.pl?biblionumber=169210

Akhmedsafin, U., Mirlas, V., S. V., Shestakov, F., Krashin, I., & Shin, G. (1982). *Hydro-geological models of inermountane artesian basins: Alma-Ata*. Nauka.

Akhmedsafin, U., Mirlas, V., Shlygina, V., Shestakov, F., Malahov, V., & Vitvitskay, L. (1980). *Ily artesian basin: Alma-Ata*. Nauka.

Alemie, T. C., Tilahun, S. A., Ochoa-Tocachi, B. F., Schmitter, P., Buytaert, W., Parlange, J. Y., & Steenhuis, T. S. (2019). Predicting shallow groundwater tables for sloping highland aquifers. *Water Resources Research*, *55*(12), 11088–11100. https://doi.org/10.1029/2019WR025050

Allocca, V., Coda, S., Calcaterra, D., & De Vita, P. (2022). Groundwater rebound and flooding in the Naples' periurban area (Italy). *Journal of Flood Risk Management*, *15*(2), 1–20. https://doi.org/10.1111/jfr3.12775

Allocca, V., Di Napoli, M., Coda, S., Carotenuto, F., Calcaterra, D., Di Martire, D., & De Vita, P. (2021). A novel methodology for groundwater flooding susceptibility assessment through machine learning techniques in a mixed-land use aquifer. *Science of the Total Environment*, *790*, 148067. https://doi.org/10.1016/j.scitotenv.2021.148067

Anker, Y., Mirlas, V., Gimburg, A., Zilberbrand, M., Nakonechny, F., Meir, I., & Inbar, M. (2019). Effect of rapid urbanization on Mediterranean karstic mountainous drainage basins. *Sustainable Cities and Society*, *51*, 101704. https://doi.org/10.1016/j.scs.2019.101704

Azarafza, M., & Ghazifard, A. (2016). Urban geology of Tabriz City: Environmental and geological constraints. *Advances in Environmental Research*, *5*(2), 95–108. https://doi.org/10.12989/aer.2016.5.2.095

Ball, T., Werritty, A., & Geddes, A. (2013). Insurance and sustainability in flood-risk management: The UK in a transitional state. *Area*, *45*(3), 266–272. https://doi.org/10.1111/area.12038

Bovolenta, R., & Bianchi, D. (2020). Geotechnical analysis and 3D FEM modeling of Ville San Pietro (Italy). *Geosciences*, *10*(11), 1–23. https://doi.org/10.3390/geosciences10110473

Chebanov, O., & Zadniprovska, A. (2011). *Zoning groundwater flooding risks in the cities and urban agglomeration areas of Ukraine* (pp. 71–76). IAHS-AISH Publication.

Cherednichenko, A., Cherednichenko, A., Vilesov, E. N., & Cherednichenko, V. S. (2015). Climate change in the City of Àlmaty during the past 120 years. *Quaternary International*, *358*, 101–105. https://doi.org/10.1016/j.quaint.2014.12.035

Chigrinets, A. G., Mazur, L. P., Duskayev, K. K., Chigrinets, L. Y., & Akhmetova, S. T. (2019). Water economy balance of the Almaty city. *Journal of Ecological Engineering*, *20*(3), 194–203. https://doi.org/10.12911/22998993/99783

Fernández, D. S., & Lutz, M. A. (2010). Urban flood hazard zoning in Tucumán Province, Argentina, using GIS and multicriteria decision analysis. *Engineering Geology*, *111*(1–4), 90–98. https://doi.org/10.1016/j.enggeo.2009.12.006

Gao, J., Jiang, Y., & Anker, Y. (2021). Contribution analysis on spatial tradeoff/synergy of karst soil conservation and water retention for various geomorphological types. *Geographical Detector Application: Ecological Indicators*, *125*, 107470. https://doi.org/10.1016/j.ecolind.2021.107470

Google. (2021). *Almaty satellite image*. https://www.google.com/maps/place/Almaty,+Kazakhstan/@43.264053,76.8336118,2302m/data=!3m1!1e3!4m5!3m4!1s0x38836e7d16c5cbab:0x3d44668fad986d76!8m2!3d43.2220146!4d76.8512485?hl=en

Hughes, A. G., Vounaki, T., Peach, D. W., Ireson, A. M., Jackson, C. R., Butler, A. P., Bloomfield, J. P., Finch, J., & Wheater, H. S. (2011). Flood risk from groundwater: Examples from a chalk catchment in southern England. *Journal of Flood Risk Management*, *4*(3), 143–155. https://doi.org/10.1111/j.1753-318X.2011.01095.x

Kumar, P., Debele, S. E., Sahani, J., Rawat, N., Marti-Cardona, B., Alfieri, S. M., Basu, B., Basu, A. S., Bowyer, P., Charizopoulos, N., Gallotti, G., Jaakko, J., Leo, L. S., Loupis, M., Menenti, M., Mickovski, S. B., Mun, S. J., Gonzalez-Ollauri, A., Pfeiffer, J., … Zieher, T. (2021). Nature-based solutions efficiency evaluation against natural hazards: Modelling methods, advantages and limitations. *Science of the Total Environment*, *784*, 147058. https://doi.org/10.1016/j.scitotenv.2021.147058

Lara, M., & Sepúlveda, S. A. (2010). Landslide susceptibility and hazard assessment in San Ramón ravine, Santiago de Chile, from an engineering geological approach. *Environmental Earth*

1753318x, 2025, 1, Downloaded from https://onlinelibrary.wiley.com/doi/10.1111/jfr3.13029 by INASP/HINARI - KAZAKHSTAN, Wiley Online Library on [05/04/2026]. See the Terms and Conditions (https://onlinelibrary.wiley.com/terms-and-conditions) on Wiley Online Library for rules of use; OA articles are governed by the applicable Creative Commons License

Sciences, *60*(6), 1227–1243. https://doi.org/10.1007/s12665-009-0264-5

MacDonald, D., Dixon, A., Newell, A., & Hallaways, A. (2012). Groundwater flooding within an urbanised flood plain. *Journal of Flood Risk Management*, *5*(1), 68–80. https://doi.org/10.1111/j.1753-318X.2011.01127.x

Mavritskii, B. F., Shpak, A. A., Otman, N. S., Antonenko, G. F., & Grebenshchikova, T. B. (1983). Explanatory Note to the Atlas of Thermal Waters. *VSEGINGEO*. (in Russian).

Pandit, R., Parrotta, J. A., Chaudhary, A. K., Karlen, D. L., Vieira, D. L. M., Anker, Y., Chen, R., Morris, J., Harris, J., & Ntshotsho, P. (2020). A framework to evaluate land degradation and restoration responses for improved planning and. *Ecosystems and People*, *15*(1), 1–18. https://doi.org/10.1080/26395916.2019.1697756

Sanford, W. (2002). Recharge and groundwater models: An overview. *Hydrogeology Journal*, *10*(1), 110–120. https://doi.org/10.1007/s10040-001-0173-5

Schlumberger Water Services. (2011). *Visual MODFLOW 2011.1 user's manual*. https://www.academia.edu/21399537/Visual_MODFLOW_2011_1_Users_Manual_For_Professional_Applications_in_Three_Dimensional_Groundwater_Flow_and_Contaminant_Transport_Modeling_Images_created_using_Visual_MODFLOW_Premium

Skilodimou, H. D., & Bathrellos, G. D. (2020). Natural and technological hazards in urban areas: Assessment, planning and solutions. *Sustainability*, *13*(15), 8301. https://doi.org/10.3390/su13158301

Sotnikov, Y. V., & Ibraimov, V. M. (2017). Calculated water demand as the main factor influencing the reliability of hydrogeological forecasts at the evaluation of groundwater elastic reserves. *Bulletin of the National Academy Science of the Republic of Kazakhstan*, *367*(3), 13–26.

Su, X., Liu, T., Beheshti, M., & Prigiobbe, V. (2020). Relationship between infiltration, sewer rehabilitation, and groundwater flooding in coastal urban areas. *Environmental Science and Pollution Research*, *27*(13), 14288–14298. https://doi.org/10.1007/s11356-019-06513-z

Vakhshoori, V., Pourghasemi, H. R., Zare, M., & Blaschke, T. (2019). Landslide susceptibility mapping using GIS-based data mining algorithms. *Water*, *11*(11), 7–13. https://doi.org/10.3390/w11112292

Wang, J., Wah Yu, C., & Cao, S. J. (2022). Urban development in the context of extreme flooding events. *Indoor and Built Environment*, *31*(1), 3–6. https://doi.org/10.1177/1420326X211048577

Wu, C., Guo, Y., & Su, L. (2021). Risk assessment of geological disasters in Nyingchi, Tibet. *Open Geosciences*, *13*(1), 219–232. https://doi.org/10.1515/geo-2020-0208

Xiong, B., Chen, R., Xia, Z., Ye, C., & Anker, Y. (2020). Large-scale deforestation of mountainous areas during the 21st century in Zhejiang Province. *Land Degradation and Development*, *2015*, 1–14. https://doi.org/10.1002/ldr.3563

Yihdego, Y., Danis, C., & Paffard, A. (2017). Groundwater engineering in an environmentally sensitive urban area: Assessment, landuse change/infrastructure impacts and mitigation measures. *Hydrology*, *4*(3), 1–19. https://doi.org/10.3390/hydrology4030037

Zarghami, S. A., & Dumrak, J. (2021). A system dynamics model for social vulnerability to natural disasters: Disaster risk assessment of an Australian city. *International Journal of Disaster Risk Reduction*, *60*, 102258. https://doi.org/10.1016/j.ijdrr.2021.102258

Zhakyp, A. E., Mirlas, V. M., & Auelkhan, Y. S. (2021). Assessment of hazardous engineering-geological and hydrogeological processes on the Almaty City territory. *Bulletin of the Tomsk Polytechnic University. Geo Assets Engineering*, *332*(10), 45–56. https://doi.org/10.18799/24131830/2021/10/3088

Zou, L., & Gui, W. (2020). Simulation and prediction of geologic hazards and the impacts on homestay buildings in scenery spots through BIM. *PLoS ONE*, *15*(9), 1–14. https://doi.org/10.1371/journal.pone.0238864

How to cite this article: Mirlas, V., Zhakyp, A., Auelkhan, Y., & Anker, Y. (2025). Assessment of urbanization-related groundwater flooding process via Visual MODFLOW modeling: A case study for the northern part of Almaty city, Kazakhstan. *Journal of Flood Risk Management*, *18*(1), e13029. https://doi.org/10.1111/jfr3.13029

1753318x, 2025, 1, Downloaded from https://onlinelibrary.wiley.com/doi/10.1111/jfr3.13029 by INASP/HINARI - KAZAKHSTAN, Wiley Online Library on [05/04/2026]. See the Terms and Conditions (https://onlinelibrary.wiley.com/terms-and-conditions) on Wiley Online Library for rules of use; OA articles are governed by the applicable Creative Commons License